

Occupation of electron subbands in optically excited δ -acceptor-doped GaAs/Al_xGa_{1-x}As heterostructure

J. Łusakowski,^{1,*} R. Buczko,² K.-J. Friedland,³ and R. Hey³

¹*Faculty of Physics, University of Warsaw, ul. Hoża 69, PL-00-681 Warsaw, Poland*

²*Institute of Physics, Polish Academy of Sciences, Al. Lotników 32/46, PL-02-668 Warsaw, Poland*

³*Paul-Drude Institut für Festkörperelektronik, Hausvogteiplatz 5-7, DE-10117 Berlin, Germany*

(Received 23 April 2011; published 24 June 2011)

Photoluminescence (PL) measurements were carried out on a Be-acceptor δ -doped GaAs/Al_{0.33}Ga_{0.67}As heterostructure at 1.6 K at magnetic fields up to 5 T. The studied PL originated from the recombination of free electrons in a two-dimensional electron gas with holes captured on Be acceptors. The electron concentration on the first electric subband was estimated by an analysis of the evolution of Landau levels in the magnetic field. To find the concentration of electrons on the second electric subband we analyzed the PL intensity at zero magnetic field and compared it with calculations based on a spherical model of a shallow acceptor. Calculations carried out for different models of an acceptor-bound hole envelope wave function allow to discuss quantitatively the validity of approximations often used to describe free-to-bound $\Gamma_6 \rightarrow \Gamma_8$ transitions.

DOI: [10.1103/PhysRevB.83.245313](https://doi.org/10.1103/PhysRevB.83.245313)

PACS number(s): 73.20.Hb, 78.67.De

I. INTRODUCTION

The population of the second electrical subband (SES) in heterostructures and quantum wells influences many of their physical properties, which was observed in a large variety of experiments. To give a feeling of a diversity of studies related to this subject, let us present the following (nonexhaustive) list of investigations. For example, it was shown that the population of higher subbands opens new channels of electron-scattering mechanisms, which degrades the electron mobility.^{1,2} An influence of occupation of the SES on the thermopower was found in experiments on a high-electron-mobility GaAs/AlGaAs heterostructure.³ Time-resolved Kerr-rotation studies on a single GaAs/AlGaAs heterostructure⁴ showed a big difference in the spin dynamics of electrons on the first and second subbands. A strong dependence on the magnetic field (B) was observed for the effective mass of electrons on the SES in a system of two coupled quantum wells.⁵ A Fermi-energy edge singularity in the SES was investigated by photoluminescence and photoluminescence excitation spectroscopy in an asymmetric modulation-doped AlGaAs/InGaAs quantum well in connection with many-body effects in a high-density electron gas. In a GaAs/AlGaAs heterostructure with two subbands populated, a strong deviation from $1/B$ -periodic oscillations of the magnetization of a two-dimensional electron gas, typically observed in systems with only one subband occupied, were found.⁶ The attenuation of the surface acoustic waves in the quantum-Hall-effect regime was observed to be influenced by the population of the SES.⁷

One of the basic questions in this kind of investigation concerns the concentration of electrons on the SES. This quantity is usually difficult to determine, in particular, in cases when the system investigated is driven out of the thermodynamic equilibrium or the concentration on the second subband is very small. The present paper describes an approach to solve this difficulty in a single GaAs/AlGaAs heterostructure δ -doped with Be acceptors.

Before going into the details of this study, let us point out that two-dimensional GaAs/AlGaAs single heterostructures

and quantum wells doped with Be acceptors have been widely investigated both in the context of the basic physical properties as well as applications. Spectroscopic studies on Be-doped quantum wells were carried out by optical techniques to give essential information about the symmetry and energy of acceptor states spatially confined by a quantum well (see, for example, Refs. 8–12 and references therein, also a general review on optical properties of impurities in modern nanomaterials can be found in Ref. 13). The energy of transitions between Be acceptor levels, or acceptor levels split by the magnetic field, falls within mid- or far-infrared (THz) range. For this reason, quantum structures doped with Be acceptors have been used as basic components of mid-infrared and THz detectors. In particular, Be-doped multiple quantum wells are broadly used as quantum-well infrared photoconductor detectors.^{14–16} An electrostatic potential induced by a barrier-related quantum confinement is a tool that is used to tune the energy and splitting of an acceptor level and enables engineering of a detector response.

Thus, the present paper falls within two areas of interest: the physics of electrons on the second electrical subband and application of Be-doped quantum structures as detectors. The peculiarity of the system investigated in the present work is that Be acceptors are situated far enough from the GaAs/AlGaAs interface and thus can be considered as embedded in a bulk GaAs crystal. For this reason, we do not consider any quantum-confinement effect on Be acceptor levels.

The aim of this paper is to present a scheme of analysis allowing to evaluate the electron concentration on electrical subbands in an optically excited heterostructure, i.e., in a system driven to nonequilibrium conditions by a laser light. To determine the free-electron concentration, one usually performs Hall-effect, Shubnikov-de-Haas-effect, or plasma-reflectivity measurements. These techniques are not reliable if the investigated sample is subjected to a local optical excitation, as it is, for instance, in the case of a photoluminescence (PL) experiment. The reason is that the concentration of carriers in the area where the laser spot is focused is usually

quite different from that in the nonilluminated part of the sample, while the methods mentioned above give only an average value of the concentration. On the other hand, this is the concentration in the optically excited area that is required to analyze the experimental data. Thus, it is of great interest to determine the electron concentration directly from the optical experiment data. One of methods was proposed by Babiński *et al.*,¹⁷ who correlated Shubnikov-de-Haas-like oscillations of a free-to-bound luminescence intensity from a GaInAs quantum well to the electron concentration on the first electrical subband. Another approach was proposed by Kukushkin and Timofeev¹⁸ and Hartmann *et al.*¹⁹ in the case of a free-to-bound transition in a single heterostructure doped with shallow acceptors.

In the present paper, we develop ideas presented in Refs. 18 and 19 by considering PL experiments carried out on a single GaAs/AlGaAs heterostructure with a δ layer of Be acceptors introduced at 30 nm from the GaAs/AlGaAs interface into the GaAs channel. A two-dimensional gas of free electrons (2DEG), which resides at the interface, appears due to doping of the AlGaAs barrier with shallow donors. At liquid-helium temperatures, which are of interest here, and in the dark, only the first electric state of the heterostructure quantum well is occupied. However, an optical excitation with a laser beam during a PL experiment leads to a nonequilibrium population of the second electric subband, which is evidenced in PL spectra.

Although a PL originating from the recombination of electrons on the *second* subband with holes in the δ layer was always clearly observed, the Landau quantization of the SES was not reported.^{18–20} The electron concentration on the SES was determined in Ref. 19 only at strong magnetic fields, corresponding to $\nu < 1$. Let us note, however, that a possible drawback of such an approach comes from a strong localization of electrons induced by the magnetic field that can essentially reduce the free-electron concentration. In the present paper, we apply the idea of Ref. 19 to determine the electron concentration on the SES (n_2) by considering the ratio of PL intensity originating from the first and the second subbands (I_1 and I_2 , respectively). There are, however, important differences between the present approach and that of Ref. 19. First, the ratio analyzed, I_2/I_1 , is determined at zero magnetic field ($B = 0$), and not at high B . Second, we use an essentially more realistic model to describe the electron and hole wave functions. We took explicitly into account the $L = 2$ part of the hole envelope part as well as the nonzero k vector of free electrons that were neglected in previous studies.^{18,19} We show that at a weak optical excitation of the heterostructure investigated, the electron concentration on the second subband, $n_2 \approx (4 \pm 1) \times 10^9 \text{ cm}^{-2}$, is really too small to allow observation of the Landau quantization. Considering a more advanced model of the acceptor envelope wave function we were able to show conditions when approximations resulting from a simpler approach based on a Bohr model of a shallow acceptor are justified.

The paper is organized as follows. The sample investigated, the experimental techniques, and the results are presented in Sec. II. Section III describes a theoretical model of the electric-dipole optical transitions in-

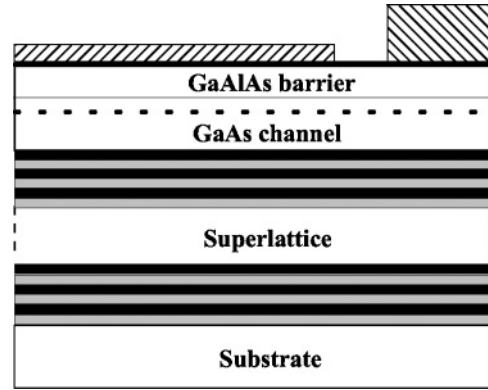


FIG. 1. A structure of the sample investigated (not to scale). A Be δ layer is marked by a dotted line. A semitransparent gate (top left) and an ohmic contact (top right) are shown with hatched rectangles. A GaAs cap on the top of AlGaAs barrier is indicated with a thick line.

cluding a 2DEG electron and an acceptor bound hole. The results are discussed in Sec. IV and concluded in Sec. V.

II. EXPERIMENT AND RESULTS

The sample under investigation was a high-quality GaAs/Al_{0.33}Ga_{0.67}As heterostructure grown on a semi-insulating GaAs substrate (see Fig. 1). The GaAs channel of about 1 μm above 50 periods of a 5-nm/5-nm GaAs/AlAs superlattice contains unintentional acceptors at a concentration less than 10^{14} cm^{-3} . The AlGaAs barrier comprises an undoped 45-nm-thick AlGaAs spacer and a uniformly Si-doped 35-nm-thick AlGaAs layer; the doping level amounts to 10^{18} cm^{-3} . A δ layer of Be atoms with a concentration of 10^9 cm^{-2} was introduced into the GaAs channel at the distance $z_0 = 30 \text{ nm}$ away from the GaAs/AlGaAs interface. Based on the growth conditions, the width of the δ layer is estimated to be one atomic layer. The barrier of the structure was covered with a 15-nm-thick GaAs cap layer.

The measurements were carried out in an optical helium cryostat supplied with a split coil; the magnetic field was perpendicular to the 2DEG layer. All measurements were carried out at $1.60 \pm 0.03 \text{ K}$. The luminescence was excited by a He-Ne laser. If not stated differently, all data presented in this paper were obtained in one experimental run at the same excitation power of about 10 mW/cm^2 . The luminescence was analyzed with a spectrometer supplied with a charge-coupled-device (CCD) camera. A semitransparent Au gate electrode and an ohmic contact were fabricated on the sample surface and the concentration of the 2DEG was tuned by polarizing the gate with a voltage source.

A scheme of the heterostructure energy band structure in the vicinity of the GaAs/AlGaAs interface is shown in Fig. 2, which gives also an idea about optical transitions expected in the investigated heterostructure. To preserve a clarity of the figure we do not indicate all possible transitions, like donor- or acceptor-bound excitons or optical transitions in the AlGaAs barrier.

An overall shape of the PL spectrum in a broader range of energy is shown in the inset to Fig. 3. There are two clearly

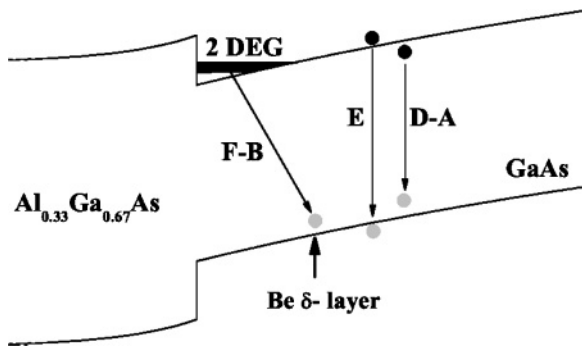


FIG. 2. A scheme of the band structure of the GaAs/AlGaAs heterostructure. Dark (grey) dots mimic electrons (holes). A Be δ layer is marked with a short vertical arrow. Some of the possible optical transitions are indicated: free-exciton recombination (E), donor-acceptor recombination (D-A), and 2DEG electron-hole localized on a Be acceptor in the δ layer (F-B; free-to-bound).

separated parts of the spectrum: a lower-energy part around 1.49 eV, which is related to 2DEG Be-acceptor-bound-hole recombination (F-B transition in Fig. 2), and a higher-energy one around 1.50–1.51 eV, which is related to band-to-band transitions involving free (the arrow E in Fig. 2) and bound excitons. Since the high-energy part of the spectrum was of no interest in the present investigation, we did not carry out either its detailed analysis or identification of constituent lines. In the present paper, we concentrate only on transitions between electrons in the 2DEG and holes bound to acceptors in the δ layer.

A luminescence originating from recombination of free electrons with an acceptor bound hole in the δ layer can be masked with a broad structure of donor-acceptor transitions. We avoided this problem by keeping the power of the laser excitation on a very low level of a few mW/cm^2 . Examples of the corresponding data are shown in Fig. 3; at such low excitation powers, no additional features appear in spectra when the power is changed. What is only observed is a shift

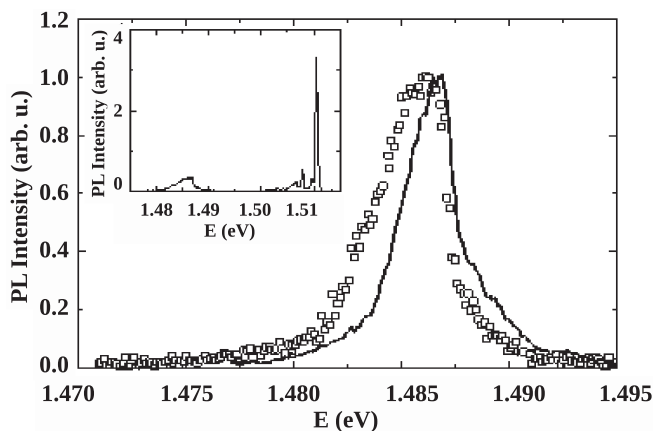


FIG. 3. PL spectrum of 2DEG Be-acceptor-bound-hole transitions for the excitation power of 5 (open squares) and 10 mW/cm^2 (solid line). The spectra are normalized to their maximum. Inset: PL spectrum involving band-to-band transitions (at about 1.50–1.51 eV) and recombination between 2D electrons and holes bound in the Be δ layer (at about 1.49 eV).

of the line and its shrinkage with increasing excitation power, which reflects changes in 2DEG concentration, and agrees with previous studies.¹⁸ Another experimental proof of a negligible role of donor-acceptor transitions is that spectra at the magnetic field, showing a few well-resolved Landau levels, could always be simulated with a sum of Lorentzians only, with their number corresponding to the number of peaks in the spectrum, without any additional background level.

Following Ref. 18, to determine the electron concentration on the first electric subband n_1 we considered a PL originated from a radiative recombination of 2DEG with optically excited holes captured in the δ layer and we analyzed the influence of the magnetic field on PL spectra. In the magnetic field, the density of states of the 2DEG is quantized into Landau levels and a PL spectrum is composed of a number of peaks, numbered with $N = 0, 1, \dots$, see Fig. 4. A peak with a given N corresponds to the recombination of electrons on the N th Landau level with holes captured on acceptors. Since the degeneracy of Landau levels grows with B , the number of peaks in PL spectra decreases with increasing B . Tracing the evolution of the spectra with the magnetic field, one can determine the values of B at which luminescence from Landau levels with a given N disappears. This defines the magnetic field corresponding to the filling factor, $\nu = 2(N + 1)$, and thus allows to estimate the concentration of the 2DEG. Typically, one concentrates on the magnetic field $B_{\nu=2}$ (or $B_{\nu=4}$) since this can be determined with a high precision. Knowing the degeneracy of Landau levels and the value of $B_{\nu=2}$ one can determine $n_1 = 2B_{\nu=2}/(h/2e)$, where h is the Planck constant and e is the electron charge. Experiments show that $B_{\nu=2}$ can be determined with a precision of 0.1 T, which limits the method to electric subbands with an electron concentration higher than about 10^{10} cm^{-2} (at which $\Delta n_1 \sim n_1$).

An evolution of PL spectra with the magnetic field, like that shown in Fig. 4, was used to determine the electron

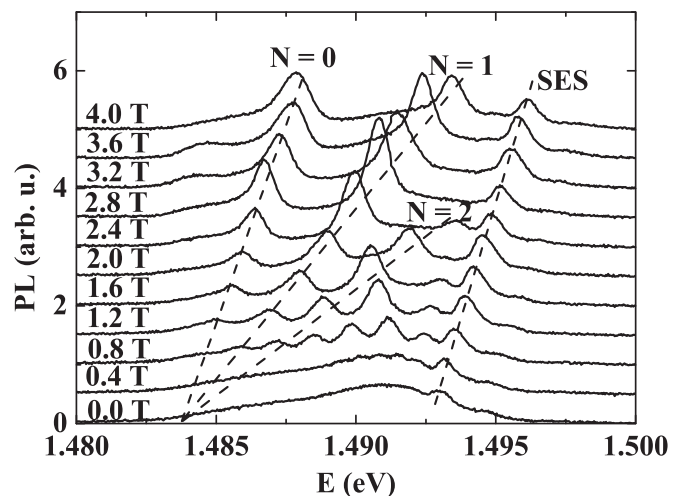


FIG. 4. Evolution of PL spectra as a function of B from 0 to 4 T every 0.4 T for $n_1 = 2.6 \times 10^{11} \text{ cm}^{-2}$. Dashed lines are guides for the eye and indicate PL peaks originating from the second electric subband (SES) and $N = 0, 1, 2$ Landau levels of the first electric subband. A spectrum for $B = 0.8$ T shows also peaks corresponding to $N = 3, 4, 5$, and for $B = 1.2$ T peaks corresponding to $N = 3$ and 4, and for $B = 1.6$ T, a peak corresponding to $N = 3$.

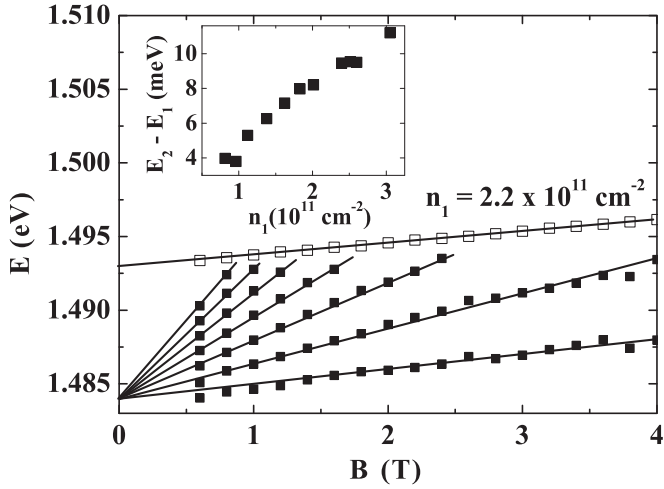


FIG. 5. Position of the PL peak from the second electrical subband (open squares) and PL peaks from Landau levels of the first subband (full squares) as a function of the magnetic field B at $n_1 = 2.2 \times 10^{11} \text{ cm}^{-2}$. Solid lines: linear fit to experimental data. Inset: experimentally determined $E_2 - E_1$ as a function of experimentally determined n_1 .

concentration n_1 for all gate polarizations applied, and also to determine the energy of the bottom of the first and second electric subbands (E_1 and E_2 , respectively). An example of this procedure in the case of $n_1 = 2.2 \times 10^{11} \text{ cm}^{-2}$ is shown in Fig. 5. The energies E_1 and E_2 are determined by intersection of linear fits (solid lines in Fig. 5) with the energy axis. Also, one can notice that in this case $B_{\nu=4} \approx 2.4 \text{ T}$. Since PL spectra were measured each 0.2 T, the precision of estimation of n_1 is equal to about $2 \times 10^{10} \text{ cm}^{-2}$.

Figure 6 shows an evolution of the luminescence spectrum at $B = 0$ as a function of n_1 . The spectra are normalized to the maximum of the signal. An increase of the relative intensity of the luminescence from the second subband is evident.

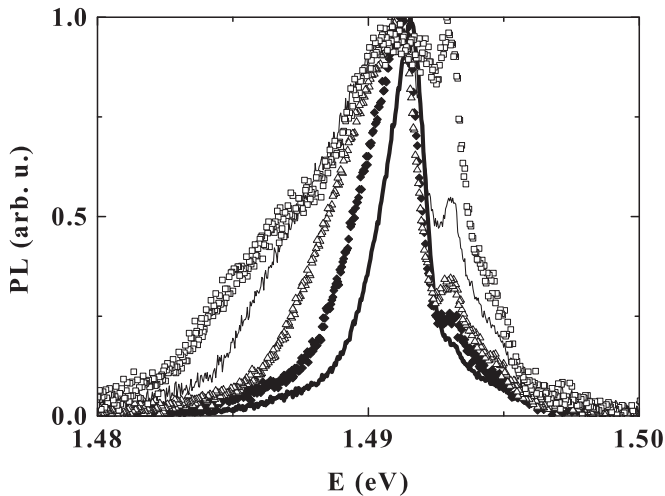


FIG. 6. Evolution of the shape of the PL spectrum at $B = 0$ as a function of n_1 equal to (in units of 10^{11} cm^{-2}) 1.0 (thick solid line), 1.3 (diamonds), 1.6 (triangles), 2.2 (thin solid line), and 2.8 (open squares). The sharp structure centered at about 1.493 eV is the PL from the second subband.

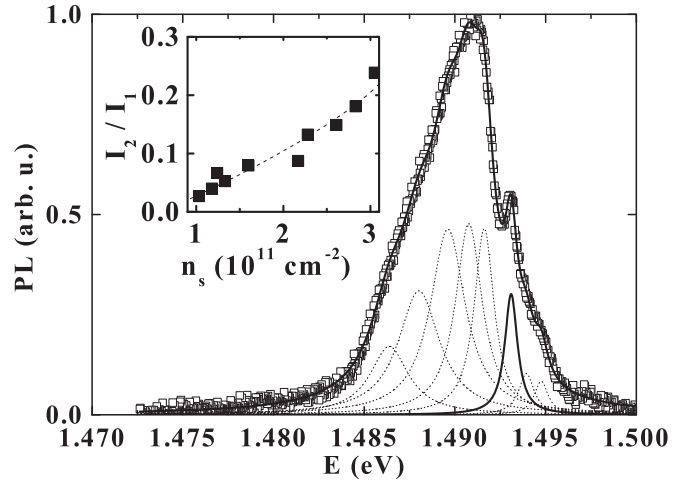


FIG. 7. Deconvolution of a luminescence spectrum at $B = 0$ and $n_1 = 2.2 \times 10^{11} \text{ cm}^{-2}$ into Lorentzians. Identification of spectral features is the same as in the Fig. 6. Inset: Experimentally determined I_2/I_1 as a function of n_1 (points), where I_2 and I_1 were calculated as the area of the corresponding structures in spectra, like that shown in the figure main body. Dashed line is guide to the eye.

The width of the spectra increases as n_1 grows, reflecting an increasing concentration of the 2DEG.

Each spectrum measured at $B = 0$ was deconvoluted to determine signals originating from the first and the second subband. An example is shown in Fig. 7 for $n_1 = 2.2 \times 10^{11} \text{ cm}^{-2}$. The spectra were deconvoluted into Lorentzians. The number of peaks was adapted for each spectrum separately to reproduce precisely its shape. The signal originating from the second subband was always described by a single peak (thick solid line in Fig. 7). With the shape of a spectrum well reproduced, the area of the peak corresponding to the second subband is essentially independent of the number of peaks used to describe the PL from the first subband. This results from the fact that the PL from the second subband is a clearly defined and strong feature in the spectra.

III. THE MODEL

The first task here is to calculate matrix elements of optical transitions to determine the I_2/I_1 ratio observed in the experiment. A detailed description of calculations is given below to underline the essential difference of the present approach and the simplified picture adopted previously,^{18,19} which neglected both the $L = 2$ part of the acceptor envelope wave function and the in-plane electron wave vector. Application of this model in the case of a nonzero magnetic field and the first subband, was described in Ref. 20. Here, the calculations are carried out for zero magnetic field and both the first and second electric subbands.

Let us denote the electron envelope wave function in the n th subband as $c_n(z) \exp(i\mathbf{k}\boldsymbol{\rho})$, where $n = 1$ and 2. Functions $c_n(z)$ result from self-consistent calculations of the electrostatic potential (a temperature of 1.6 K was assumed in these calculations). The z axis is perpendicular to the 2DEG plane; $z = 0$ corresponds to the position of the GaAs/AlGaAs interface. Vectors \mathbf{k} and $\boldsymbol{\rho}$ are, respectively, the electron wave vector and position in the xy plane where the 2DEG

resides. The periodic part of the electron wave function, $u_{j=\frac{1}{2},j_z} = |R_0, \frac{1}{2}, j = \frac{1}{2}, j_z\rangle$, corresponds to the total angular momentum equal to $j = \frac{1}{2}$, and it is composed of s -like functions (denoted as R_0) and $\frac{1}{2}$ spinors. Thus, the electron functions are $\langle \mathbf{r} | n, \mathbf{k}, j_z \rangle = c_n(z) \exp(i\mathbf{k}\boldsymbol{\rho}) \langle \mathbf{r} | R_0, \frac{1}{2}, \frac{1}{2}, j_z \rangle$.

Since a spatial extension of a Be-acceptor wave function is much smaller than the distance of the acceptor δ layer to the GaAs/AlGaAs interface, we can consider an acceptor as embedded in a bulk GaAs. Then, the hole wave function is described within the spherical model of the acceptor²⁵ as

$$\begin{aligned} \langle \mathbf{r} | \frac{3}{2}, F_z \rangle &= f_0(r) \langle \mathbf{r} | L = 0, J = \frac{3}{2}, F = \frac{3}{2}, F_z \rangle \\ &+ f_2(r) \langle \mathbf{r} | L = 2, J = \frac{3}{2}, F = \frac{3}{2}, F_z \rangle, \end{aligned}$$

where $f_0(r)$ and $f_2(r)$ are radial functions, which are expressed as a sum of exponents, and are numerically calculated.²⁵ The functions $|L, J = \frac{3}{2}, F = \frac{3}{2}, F_z\rangle$ are superpositions of spherical harmonics Y_{LM} ($|M| \leq L$) and p -type periodic functions $u_{J=\frac{3}{2},j_z} = |R_1, \frac{1}{2}, J = \frac{3}{2}, j_z\rangle$. The latter functions are, in turn, built with sp^3 orbitals R_1 and the spin $\frac{1}{2}$. We choose the basis:

$$\begin{aligned} u_{J=\frac{3}{2},\frac{3}{2}} &= -\frac{1}{\sqrt{2}}(X + iY)\alpha, \\ u_{J=\frac{3}{2},\frac{1}{2}} &= -\frac{1}{\sqrt{6}}[(X + iY)\beta - 2Z\alpha], \\ u_{J=\frac{3}{2},-\frac{1}{2}} &= \frac{1}{\sqrt{6}}[(X - iY)\alpha + 2Z\beta], \\ u_{J=\frac{3}{2},-\frac{3}{2}} &= \frac{1}{\sqrt{2}}(X - iY)\beta, \end{aligned}$$

where X , Y , and Z are functions transforming as x , y , and z under operations of the T_d symmetry group, respectively.

At $B = 0$, the luminescence can be considered as composed of an equal number of photons of both circular polarizations. For this reason, we calculate matrix elements of optical transitions corresponding to the operator $\hat{p}_{1,\pm 1} = \mp(\hat{p}_x \pm i\hat{p}_y)$, where \hat{p}_x and \hat{p}_y are components of the momentum operator. The interband matrix element of the operator $\hat{p}_{1,\pm 1}$ in the Γ point is

$$\begin{aligned} &\left\langle R_0, \frac{1}{2}, \frac{1}{2}, j_z \left| \hat{p}_{1,\pm 1} \right| R_1, \frac{1}{2}, \frac{3}{2}, J_z \right\rangle \\ &= -\sqrt{\frac{3}{2}} C_{\frac{3}{2},\frac{3}{2},\frac{1}{2},1,\pm 1}^{\frac{1}{2},j_z} \begin{Bmatrix} 1 & \frac{1}{2} & \frac{3}{2} \\ \frac{1}{2} & 1 & 0 \end{Bmatrix} \langle R_0 \| \hat{p}_1 \| R_1 \rangle = C_{\frac{3}{2},\frac{3}{2},\frac{1}{2},1,\pm 1}^{\frac{1}{2},j_z} p, \end{aligned} \quad (1)$$

where C is the Clebsch-Gordan coefficient and p is a constant. Let us consider the following matrix elements:

$$\begin{aligned} \langle n, \mathbf{k}, j_z \left| \hat{p}_{1,\pm 1} \right| \frac{3}{2}, F_z \rangle &= \sum_{L=0,2} \langle n, \mathbf{k}, j_z \left| \hat{p}_{1,\pm 1} f_L \right| L, \frac{3}{2}, \frac{3}{2}, F_z \rangle \\ &= \sum_{L=0,2} \sum_{M=-L}^L C_{L,M,\frac{3}{2},J_z=F_z-M}^{\frac{3}{2},F_z} \\ &\quad \times \left\langle R_0, \frac{1}{2}, \frac{1}{2}, j_z \left| \hat{p}_{1,\pm 1} \right| R_1, \frac{1}{2}, \frac{3}{2}, J_z \right\rangle \\ &= F_z - M \int c_n^*(z_0 + z) \exp(-i\mathbf{k}\boldsymbol{\rho}) \end{aligned}$$

$$\begin{aligned} &\times f_L(r) Y_{LM}(\vartheta, \varphi) d^3r \\ &= \sum_{L=0,2} \sum_{M=-L}^L C_{L,M,\frac{3}{2},F_z-M}^{\frac{3}{2},F_z} C_{\frac{3}{2},F_z-M,1,\pm 1}^{\frac{1}{2},j_z} p \\ &\quad \times \int c_n^*(z_0 + z) \exp(-i\mathbf{k}\boldsymbol{\rho}) \\ &\quad \times f_L(r) Y_{LM}(\vartheta, \varphi) d^3r. \end{aligned} \quad (2)$$

The integrals are calculated in a coordinate system centered on the acceptor at the distance $z_0 = 30$ nm from the interface, which explains the new z argument of $c^*(z_0 + z)$ in the integrand.

Due to the cylindrical symmetry of our problem, calculations of matrix elements are easier to carry out with electron envelope functions of the cylindrical symmetry. Let ϕ be the angle determined by the direction of the \mathbf{k} vector in the xy plane. It is convenient to use the following superpositions of states $|n, \mathbf{k}, j_z\rangle$: $|n, k, m, j_z\rangle = \frac{1}{\sqrt{2\pi}} \int e^{im\phi} |n, \mathbf{k}, j_z\rangle d\phi$. It shows a cylindrical symmetry with $m\hbar$ and $j_z\hbar$ being the angular momentum projections on the z axis of envelope and Bloch parts of wave function, respectively. The total angular-momentum projection is equal to $(m + j_z)\hbar$.

Finally, the matrix elements of $\langle n, k, m, j_z \left| \hat{p}_{1,\pm 1} \right| \frac{3}{2}, F_z \rangle$ can be calculated using Eq. (2) and the integral value $\frac{1}{\sqrt{2\pi}} \int e^{-im\phi} e^{-ik\rho \cos(\phi-\varphi)} d\phi = \sqrt{2\pi} e^{-im\varphi} J_m(k\rho)$, where φ defines the direction of the vector $\boldsymbol{\rho}$. Using the identity $Y_{LM}(\vartheta, \varphi) = \varepsilon \sqrt{\frac{(2L+1)(L-|M|)!}{4\pi(L+|M|)!}} P_L^M(\cos\vartheta) e^{iM\varphi}$ [$\varepsilon = (-1)^M$ for $M > 0$ and $\varepsilon = 1$ for $M \leq 0$] we get

$$\begin{aligned} \langle n, k, m, j_z \left| \hat{p}_{1,\pm 1} \right| \frac{3}{2}, F_z \rangle &= p \sum_{L=0,2} C_{L,m,\frac{3}{2},F_z-m}^{\frac{3}{2},F_z} C_{\frac{3}{2},F_z-m,1,\pm 1}^{\frac{1}{2},j_z} \varepsilon \\ &\quad \times \sqrt{\frac{(2L+1)(L-|m|)!}{4\pi(L+|m|)!}} (2\pi)^{\frac{3}{2}} \\ &\quad \times \int c_n^*(z_0 + r \cos\vartheta) P_L^m(\cos\vartheta) J_m \\ &\quad \times (kr \sin\vartheta) f_L(r) dr d\cos\vartheta. \end{aligned} \quad (3)$$

IV. RESULTS AND DISCUSSION

Based on the above considerations one can analyze quantitatively the transitions considered. Let us first turn the attention to the selection rules. Nonzero matrix elements are for $m = F_z \pm 1 - j_z$, provided $|m| \leq 2$. The allowed transitions are shown in Fig. 8(b) and are compared to the case when the acceptor envelope function is described with the $L = 0$ part only in Fig. 8(a). In Fig. 8, the hole states are described by F_z (which is equal to J_z in the case $L = 0$), and the electron states by j_z . For readers' convenience, in the case of $L = 0, 2$ we indicated also the J_z components of each hole state with a given F_z . We stress that the selection rules shown in Fig. 8 are given for the $B = 0$ case and splitting of levels is introduced *only* to show levels of different quantum numbers.²¹

We assume that the electron concentration on the first and second subbands is equal to n_1 and n_2 , respectively. The value of n_1 was experimentally determined with the

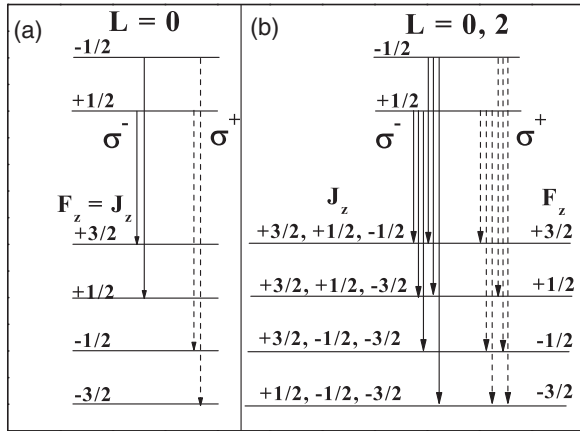


FIG. 8. Selection rules for the $\Gamma_6 \rightarrow \Gamma_8$ free-to-bound transition. Solid lines show σ^- polarization and dashed lines σ^+ polarization. An acceptor-bound-hole envelope wave function is composed of (a) the $L = 0$ part only or of (b) both the $L = 0$ and $L = 2$ parts. The figure is plotted for the $B = 0$ case; levels are split for clarity only.

procedure described in Sec. I. The intensity I_1 was numerically calculated as

$$\int_0^{k_F} \sum_{m, j_z, F_z, \mu} \left| \left\langle n_1, k, m, j_z \mid \hat{p}_{1, \mu} \left[\frac{3}{2}, F_z \right] \right\rangle \right|^2 dk, \quad (4)$$

where the matrix elements are given by Eq. (3) with a corresponding envelope $c_1(z)$ and the Fermi wave number $k_F = \sqrt{2\pi n_1}$. Since the concentration n_2 is not known, the intensity I_2 was calculated with an appropriate envelope $c_2(z)$ as a function of the maximum wave number $k_{\max} = \sqrt{2\pi n_2}$. We assume here that electrons in the second subband occupy all states with $0 < k < k_{\max}$; this assumption will be discussed below. The task now is to choose the correct value of k_{\max} . This problem was solved graphically with the help of Fig. 9. In this figure, I_2/I_1 is simultaneously plotted as a function of $k_F(n_1)$ (experimental points) and as a function of k_{\max} (solid lines) at four values of n_1 . The correct value of k_{\max} at a given n_1 is found by “putting” an experimentally measured (more precisely, extrapolated) value on an appropriate curve, which is represented with horizontal arrows. This value of k_{\max} is used next to calculate n_2 . One can notice that the value of n_2 is essentially independent of n_1 and equal to about $(4 \pm 1) \times 10^9 \text{ cm}^{-2}$ (with $k_{\max} = 1.5 \times 10^{-4} \text{ \AA}^{-1}$). The assumption of occupation of all states in the second subband up to k_{\max} implies that the intersubband relaxation is much faster than processes that reduce n_2 . In fact, we checked in time-resolved measurements that the decay time of PL from the second subband is equal to about 200 ns while the intersubband relaxation due to the emission of phonons is expected to occur on a ps time scale. In such conditions, the occupation of the second subband is determined mainly by the optical excitation power (which was kept constant during all the experiments) and is not related to the population of the first subband.

Let us explain the error of the estimation of n_2 . We assume that the numerical procedures applied give exact results for the I_2/I_1 ratio within the theoretical models used. The wave vector k_F is determined with the precision of

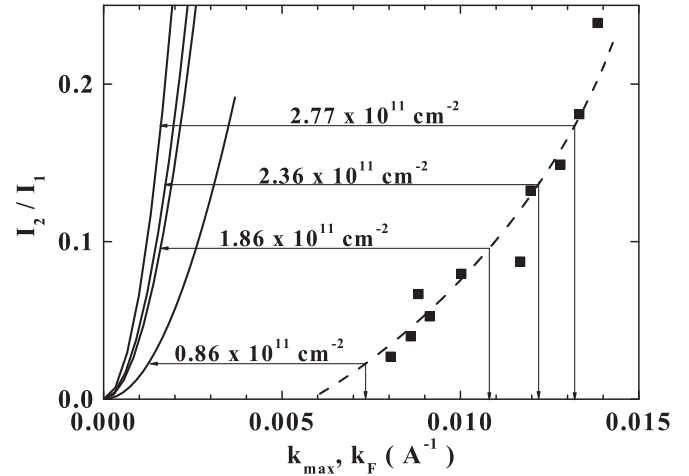


FIG. 9. Calculated (lines) and measured (points) ratio I_2/I_1 as a function of the wave number. Solid lines: I_2/I_1 as a function of k_{\max} at n_1 equal to (left to right) 2.8, 2.4, 1.9, and 0.9 (in units of 10^{11} cm^{-2}). Points: experimental values of I_2/I_1 plotted as a function of $k_F(n_1)$. Dashed line is a polynomial fit. Vertical arrows show the k_F corresponding to a given n_1 . Horizontal arrows indicate the position of an experimentally determined value on a calculated curve.

$\Delta k_F = \sqrt{2\pi/n_1} \Delta n_1$, which changes between 5×10^{-4} and $8 \times 10^{-4} \text{ \AA}^{-1}$ with $\Delta n_1 = 10^{10} \text{ cm}^{-2}$. The uncertainty of k_F related to the scatter of I_2/I_1 points in Fig. 9 can be estimated to be $5 \times 10^{-4} \text{ \AA}^{-1}$, which gives a total uncertainty of k_F of about 10^{-3} \AA^{-1} . As one can notice in Fig. 9, the corresponding uncertainty of k_{\max} is smaller due to a steep I_2/I_1 dependence on k_{\max} —we estimate it to be $2 \times 10^{-4} \text{ \AA}^{-1}$, which finally gives $\Delta n_2 = 10^9 \text{ cm}^{-2}$.

The model developed in Sec. III allowed us to calculate matrix elements of all the transitions indicated in Fig. 8 as a function of the electron wave vector, but a detailed analysis of this large amount of data is beyond the scope of the

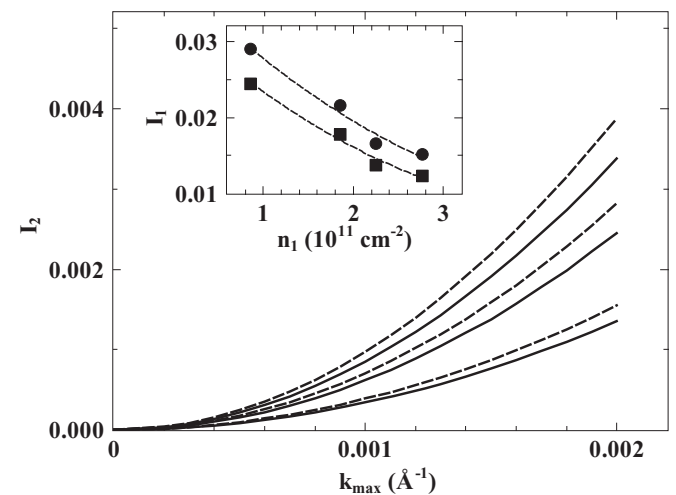


FIG. 10. Intensity I_2 calculated within the spherical $L = 0$ and 2 model (solid lines) and the Bohr model (dashed lines) of the acceptor envelope function. The three pairs of curves are for $n_1 = 0.9, 1.9,$ and 2.8 (in units of 10^{11} cm^{-2} , bottom to top). Inset: intensity I_1 as a function of concentration n_1 for the $L = 0$ and 2 model (squares) and the Bohr model (dots). Dashed lines are guide to the eye.

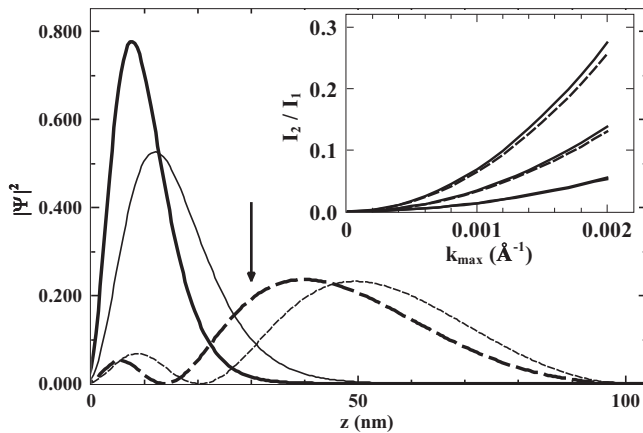


FIG. 11. Electron density corresponding to the envelope functions of the first (solid lines) and second (dashed lines) subbands for $n_1 = 0.9 \times 10^{11}$ (thin lines) and $2.8 \times 10^{11} \text{ cm}^{-2}$ (thick lines). The arrow shows the position of the δ -acceptor layer at 30 nm from the GaAs/AlGaAs interface. Inset: I_2/I_1 calculated within the $L = 0$ and 2 model (solid lines) and the Bohr model (dashed lines) for $n_1 = 0.9, 1.9,$ and 2.8 (in units of 10^{11} cm^{-2} , bottom to top).

present paper. We would like to mention only one remarkable feature resulting from taking into account the $L = 2$ part of the acceptor wave function that concerns the intensity of transitions. Let us consider the σ^- transitions indicated in Fig. 8(a) for the $L = 0$ case. Due to the symmetry imposed by the $L = 0$ approximation, the intensity of $1/2 \rightarrow 3/2$ is three times larger than that of $-1/2 \rightarrow 1/2$ (the same is true for $-1/2 \rightarrow -3/2$ and $1/2 \rightarrow -1/2$ transitions for σ^+ polarization). We have found that within the $L = 0$ and 2 approximation, the *relative* intensity of these transitions strongly depends on the electron concentration and decreases to about 1.6 at $n_1 = 2.8 \times 10^{11} \text{ cm}^{-2}$.²⁶

It appears, however, that the *total* intensities I_1 and I_2 depend relatively weakly on the acceptor-wave-function model assumed. To show this, we compare in Fig. 10 the intensities calculated within the $L = 0$ and 2 spherical model and the Bohr model of the acceptor. In the latter case, the acceptor envelope wave function was assumed to be $(\pi a_B^3)^{-1/2} \exp(-r/a_B)$, with the Bohr radius $a_B = 20 \text{ \AA}$, which corresponds to the ionization energy of a Be acceptor in GaAs.^{12,22,23} The

intensities shown in Fig. 10 calculated within the $L = 0$ and 2 model are equal to about 85% of the corresponding values obtained for the Bohr model. Since this value is approximately independent of the concentrations n_1 and n_2 , the ratio I_2/I_1 is approximately the same within the two models, as it is shown in the inset to Fig. 11.

The dependence of the intensity on the band population can be understood with the help of Fig. 11, which shows the distribution of the electron density related to the envelope wave functions in the first and second subbands. An increase of the concentration in the first subband is related to a sharpening of the shape of a triangle heterostructure quantum well and a corresponding narrowing of the electron-density distribution. Then, for the first subband, an overlap of the electron and hole envelope wave functions decreases, which results in a decrease of I_1 with n_1 . In the case of the second subband, the increase of the concentration is related to a shift of the maximum of the electron distribution toward the acceptor position, which gives an increase of I_2 with n_1 .

V. CONCLUSIONS

We carried out PL measurement on an acceptor- δ -doped GaAs/AlGaAs heterostructure at 1.6 K as a function of the 2DEG concentration. The intensities of optical transitions involving electrons on the first and second electric subbands and holes localized in δ -layer acceptors were calculated and their ratio was compared with experimentally determined values. The calculations involved self-consistent calculations of the electron wave functions and calculations of the acceptor wave function within the spherical model by taking into account both $L = 0$ and $L = 2$ parts of the envelope function. Results of the calculations were compared with experimental data, which allowed to determine the concentration of photoexcited electrons on the second electron subband. In this way, we propose an all-optical method to determine a nonequilibrium concentration of optically excited electrons on the second electron subband. We compared also results of the calculations within the $L = 0$ and 2 model with calculations based on a Bohr model of the acceptor wave function with the Bohr radius equal to 20 \AA . We showed that the results are only weakly sensitive to the model of the wave function assumed, in spite of an important difference in the scheme of selection rules valid for these two cases.

*jerzy.lusakowski@fuw.edu.pl

¹H. L. Stormer, A. C. Gossard, and W. Wiegmann, *Solid State Commun* **41**, 707 (1982).

²J. Siwiec-Matuszczyk, M. Baj, A. Babiński, and J. Kasprzak, *Acta Phys. Pol. A* **110**, 337 (2006).

³R. Fletcher, J. J. Harris, and C. T. Foxon, *Semicond. Sci. Technol.* **6**, 54 (1991).

⁴F. Zhang, H. Z. Zheng, Y. Ji, J. Liu, and G. R. Li, *Europhys. Lett.* **83**, 47007 (2008).

⁵I. Lo, J. K. Tsai, P. C. Ho, W. J. Yao, C. H. Chang, J.-C. Chiang, L.-W. Tu, and Q. X. Zhao, *Phys. Rev. B* **67**, 195317 (2003).

⁶M. R. Schaapman, U. Zeitler, P. C. M. Christianen, J. C. Maan, D. Reuter, A. D. Wieck, D. Schuh, and M. Bichler, *Phys. Rev. B* **68**, 193308 (2003).

⁷Y. Takagaki, E. Wiebicke, K.-J. Friedland, and K. H. Ploog, *Semicond. Sci. Technol.* **16**, 144 (2001).

⁸P. O. Holtz, M. Sundaram, K. Doughty, J. L. Merz, and A. C. Gossard, *Phys. Rev. B* **40**, 12338 (1989).

⁹S. Fraizzoli and A. Pasquarello, *Phys. Rev. B* **44**, 1118 (1991).

¹⁰D. Richards, J. Wagner, H. Schneider, G. Hendorfer, M. Maier, A. Fischer, and K. Ploog, *Phys. Rev. B* **47**, 9629 (1993).

- ¹¹Q. X. Zhao, P. O. Holtz, C. I. Harris, B. Monemar, and E. Veje, *Phys. Rev. B* **50**, 2023 (1994).
- ¹²J. Kundrotas, A. Čerškus, S. Ašmontas, G. Valušis, B. Sherliker, M. P. Halsall, M. J. Steer, E. Johannessen, and P. Harrison, *Phys. Rev. B* **72**, 235322 (2005).
- ¹³R. Riera, J. L. Martin, and R. A. Rosas, *Optical properties and impurity states in nanostructured materials*, in *Handbook of Advanced Electronic and Photonic Materials and Devices: Nanostructured Materials*, edited by H. S. Nalwa (Academic Press, 2001), Vol. 6.
- ¹⁴F. Szmulowicz, T. Oogarah, J. Ehret, K. Mahalingam, H. C. Liu, S. M. Hegde, J. Solomon, D. Tomich, G. Landis, and G. J. Brown, *Phys. Rev. B* **68**, 085305 (2003).
- ¹⁵W. M. Zheng, M. P. Halsall, P. Harmer, P. Harrison, and M. J. Steer, *J. Appl. Phys.* **92**, 6039 (2002).
- ¹⁶D. Seliuta, J. Kavaliauskas, B. Čechavičius, S. Balakauskas, G. Valušis, B. Sherliker, M. P. Halsall, P. Harrison, M. Lachab, S. P. Khanna, and E. H. Linfield, *Appl. Phys. Lett.* **92**, 053503 (2008).
- ¹⁷A. Babiński, M. Potemski, and H. Shtrikman, *Appl. Phys. Lett.* **88**, 051909 (2006).
- ¹⁸I. V. Kukushkin and V. B. Timofeev, *Adv. Phys.* **45**, 147 (1996).
- ¹⁹C. Hartmann, G. Martinez, C. A. Fisher, D. W. Braun, and K. Ploog, *Phys. Rev. Lett.* **80**, 810 (1998).
- ²⁰J. Łusakowski, R. Buczko, M. Sakowicz, K.-J. Friedland, R. Hey, and K. Ploog, *J. Phys. Condens. Matter* **19**, 236205 (2007).
- ²¹In the case of a nonzero magnetic field and the $L = 0$ and 2 model, selection rules depend also on the number of the Landau level, which was discussed in detail in Ref. 20.
- ²²A. C. Ferreira, P. O. Holtz, I. Buyanova, B. Monemar, M. Sundaram, J. L. Merz, and A. C. Gossard, *Thin Solid Films* **306**, 244 (1997).
- ²³R. A. Lewis and M. Henini, *Phys. Status Solidi B* **210**, 821 (1998).
- ²⁴J. Łusakowski, K.-J. Friedland, and K. Ploog, *Solid State Commun.* **142**, 299 (2007).
- ²⁵A. Baldereschi and N. O. Lipari, *Phys. Rev. B* **8**, 2697 (1973).
- ²⁶R. Buczko, J. Łusakowski, K.-J. Friedland, R. Hey, and K. Ploog, *Acta Phys. Pol. A* **114**, 1079 (2008); An analogous result was obtained also at nonzero B , which has a direct consequence on the interpretation of the degree of circular polarization of PL measured in magnetic fields, see Ref. 20 for details.